Neural Networks and SVM-Based Classification of Leukocytes Using the Morphological Pattern Spectrum

Juan Manuel Ramirez-Cortes[1], Pilar Gomez-Gil[2], Vicente Alarcon-Aquino[3], Jesus Gonzalez-Bernal[2], and Angel Garcia-Pedrero[2]

[1] Department of Electronics
National Institute of Astrophysics, Optics and Electronics.
Luis Enrique Erro No. 1 Tonantzintla, Puebla. 72840. Mexico
jmramirez@ieee.org
[2] Department of Computational Science;
National Institute of Astrophysics, Optics and Electronics.
Luis Enrique Erro No. 1 Tonantzintla, Puebla. 72840. Mexico
pgomez@acm.org, jagonzalez@inaoep.mx,
agarciapedrero@gmail.com
[3] Department of Electronics and Computer Science, University of the Americas,
Puebla, Mexico. Santa Catarina Martir, Cholula, Puebla, 72820. Mexico
vicente.alarcon@udlap.mx

Abstract. In this paper we present the morphological operator pecstrum, or pattern spectrum, as a feature extractor of discriminating characteristics in microscopic leukocytes images for classification purposes. Pecstrum provides an excellent quantitative analysis to model the morphological evolution of nuclei in blood white cells, or leukocytes. According to their maturity stage, leukocytes have been classified by medical experts in six categories, from myeloblast to polymorphonuclear corresponding to the youngest and oldest extremes, respectively. A feature vector based on the pattern spectrum, normalized area, and nucleus - cytoplasm area ratio, was tested using a multilayer perceptron neural network trained by backpropagation, and a Support Vector Machine algorithm. Results from Euclidean distance and k-nearest neighbor classifiers are also reported as reference for comparison purposes. A recognition rate of 87% was obtained in the best case, using 36 patterns for training and 18 for testing, with a three-fold validation scheme. Additional experiments exploring larger databases are currently in progress.

1 Introduction

The use of differential counting and assessment of blood white cells morphology from bone marrow is an important source of data for clinical cytology in a wide range of pathologies in the medical fields of oncology and hematology [1-3]. In order to accomplish the analysis, an important attribute to consider in leukocytes analysis is the age of the cell, which is strongly reflected in a morphological

P. Melin et al. (Eds.): Soft Comp. for Recogn. Based on Biometrics, SCI 312, pp. 19–35.
springerlink.com

evolution of its nucleus and cytoplasm. Although the maturity of the cell is a continuous variable, white blood cells are classified into discrete classes. Because the boundaries between classes are not well-defined, there are variations of counts among experts performing the same task, or even variations of counts performed by the same person on some samples in different moments.

The leukocyte differential counting consists of the quantification of the various white blood cells populations present in peripheral blood. Even though they derive from the same progenitor cell and interact with one another, each population can be considered relatively independent in terms of maturation, function, and control mechanism. The differential count has two main objectives, the search for quantitative abnormalities in morphologically normal white blood cells populations which requires high levels of precision and accuracy, and the search for morphologic abnormalities, i.e., the identification of immature or atypical cells for diagnostic or monitoring purposes, which requires a high level of clinical sensitivity. The traditional microscopic method based on the count of 100 cells has three types of error: statistical error, distributional error owing to unequal distribution of cells in the smear, and error in identifying cells related to the subjective interpretation of the examiner.

Cytology experts have identified six categories of this type of cells, according to their maturity stage, that ordered from youngest to oldest are named: Myeloblast, promyelocyte, myelocyte, metamyelocyte, band, and polymorphonuclear leukocytes [4,5]. Some typical examples of these categories are shown in figure 1, where nucleus and cytoplasm of each cell can be easily distinguished. Myeloblast is the earliest recognizable myeloid cell, and normally it has a large round to oval nucleus. Promyelocyte is slightly larger than a myeloblast. Its nucleus, although similar to a myeloblast, shows slight chromatin condensation and less prominent nucleoli with respect to the size of the cytoplasm. Myelocytes are slightly smaller than promyelocytes and have eccentric round-oval nuclei, often flattened along one side. In a typical image of a myelocyte, the proportion of the area occupied by the nucleus with respect to the cytoplasm is about 50-50 %. Metamyelocytes (10-18μ) are slightly smaller than myelocytes. They have kidney shaped indented nuclei and relatively dense chromatin, especially along the nuclear membrane. Bands are usually characterized by a U-shaped or deeply indented nucleus. Opposite sides or lobes are of roughly equal size or diameter, and there is no nuclear constriction greater than one half of the lobe diameter. Polymorphonuclear (PMN) leukocytes or segmented neutrofiles are characterized by definite lobation with thin thread-like filaments of chromatin joining the 2-5 lobes. From the previous description of typical forms of leukocytes, we can notice that definition of characteristics to discriminate among them is not straightforward, and it involves some degree of subjectivity.

Currently, there are some specialized manufacturers which offer professional equipments to perform hematologic analysis, such as Siemens ADVIA 2120, Sysmex XE-2100, or Beckman Coulter LH 750, some of them based on multicolor flow cytometry methods for the cell identification [6,7]. In this research we explore the use of mathematical morphology as a tool to create a feature extractor

able to discriminate leukocytes through image processing techniques from microscopic cell images using a personal computer.

The automatic identification of leukocytes according to their maturity stage could be very useful in the construction of automatic systems for the classification of different kinds of leukemia, differential counting of cells, and cytology applications. For this purpose, it is required to use a feature extractor able to represent shapes and at the same time, be tolerant enough to variations among patterns due to translations and rotation of the images. An additional problem associated to the creation of automatic leukocyte recognizers is the lack of public databases of leukocytes images to use for experimentation. The published research that we have found related to this kind of problem is normally carried out using private databases, which in many cases present an unbalanced number of images with respect to classes, or have been digitized under very different conditions.

Some approaches have been recently reported for automatic image analysis applied to microscopic cell imagery. In [8] the authors present a methodology to achieve a fully automated detection and classification of leukocytes based on microscope color images identifying the following classes: Basophil, Eosinophil, Lymphocyte, Monocyte and Neutrophil. The classification process is carried out using a parallel feed-forward neural network system. The feature vector is generated using the following information: Area, perimeter, convex area, solidity, major axis length, orientation, filled area, eccentricity, ratio between the cell and nucleus areas, the nucleus' "*rectangularity*" (ratio between the perimeter of the tightest bounding rectangle and the nucleus perimeter), the cell "*circularity*" (ratio between the perimeter of the tightest bounding circle and the cell perimeter), the number of lobes, and the solidity, area and mean gray-level intensity of the cytoplasm. In [9] the authors present a combination of continuous wavelet transform and moment-based features, obtained from atomic force microscope data to represent shape information of leukocyte and erythrocyte cells at multiple resolution levels. The features are then used to discriminate between anucleate versus nucleate cell types and to distinguish cells from a fibrous environment such as a tissue scaffold or stint. The authors describe the features as invariant under operations of translation, rotation, and scaling.

In [10] the authors present a classification system based on mathematical morphology to segment white blood cells. The features extracted from the segmented images include the first and second granulometric moments of nucleus, cell area, and the peak location of the morphological pattern spectrum. The classification is carried out using the fuzzy C-means algorithm. Morphological operators have been reported also for white blood cell segmentation into nucleus and cytoplasm, using scale-space filtering, the watershed transform and granulometric analysis [11].

In this work we use the morphological operator pecstrum, or pattern spectrum, as a feature extractor of discriminating characteristics in microscopic leukocytes images for classification purposes. Pecstrum is shown to provide an excellent quantitative analysis to model the morphological evolution of nuclei in blood white cells, or leukocytes according to their maturity stage. A feature vector based on the pattern spectrum, normalized area, and nucleus - cytoplasm area ratio, was tested using a multilayer perceptron neural network trained by backpropagation, and a Support Vector Machine algorithm.

2 Image Morphology

Mathematical morphology aims to quantitatively describe operations effective for the shape of objects in an image [12,13]. Operations are described by combinations of a basic set of numerical manipulations between an image A and a small object B, called a structuring element, which can be seen as a probe that scans the image and modifies it according to some specified rule. The shape and size of B, typically much smaller than the image A, together with the specific rule, define the characteristics of the performed process.

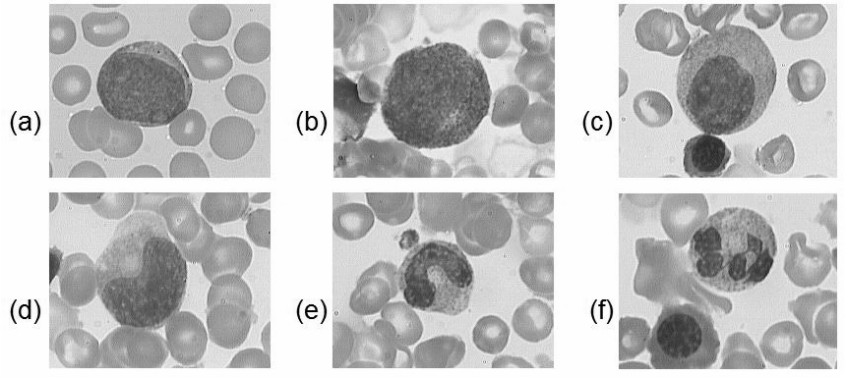

Fig. 1. Maturity stages of white blood cells. (a) Myeloblast. (b) Promyelocyte. (c) Myelocyte. (d) Metamyelocyte. (e) Band, (f) Polymorphonuclear leukocytes (PMN).

A very interesting morphological operator is the pattern spectrum or pecstrum. This operator decomposes the target image in morphological components according to the shape and size of the structuring element, providing a quantitative analysis of the morphological content of the image. Pecstrum was originally developed and reported by Maragos and Pitas [14,15]. Although it presents excellent properties as a shape extractor, with invariance to translation and rotation, pecstrum has not been extensively used, probably because it results computationally intensive in some applications, however, the available current hardware solutions easily overcome this disadvantage. The pattern spectrum has been used in the last years with several purposes: Analysis of partial discharges in high voltage systems [16], texture analysis in several applications, such as images of debris particles in polymers and composite materials [17,18], lip recognition [19], cytology of bone marrow images for the counting of white blood cells based on morphological granulometries [20], and feature extractor for hand-shape biometric applications [21]. In this work we use the pattern spectrum as a feature extractor in order to quantitatively represent the morphological evolution of the white blood cell, for cytology purposes.

2.1 Image Morphology Definitions

Binary mathematical morphology is based on two basic operators: *Dilation, and erosion*. Both are defined in terms of the interaction of the original image A to be processed, and the structuring element B. Next, both basic operators are defined. Morphological dilation is defined as the set union of the objects A obtained after the translation of the original image for each coordinate pixel *b* in the structuring element B:

$$A \oplus B = \bigcup_{b \in B} T_b(A) \tag{1}$$

Binary dilation can be interpreted as the combination of two sets by using the vector additions of set elements, called the *Minkowski Addition.* This operation is expressed as:

$$A \oplus B = \{ \mathrm{r} \mid \mathrm{r} = \mathrm{a} + \mathrm{b} \quad \forall \in \mathrm{A} \text{ and } \mathrm{b} \in \mathrm{B} \} \tag{2}$$

Morphological erosion is the morphological dual of the dilation. It is defined in terms of the Minkowski substraction as:

$$A \Theta B = \{ \mathrm{r} \mid (\mathrm{r} + \mathrm{b}) \in \mathrm{A} \, \forall \mathrm{b} \in \mathrm{B} \} \tag{3}$$

This definition can be expressed in terms of set intersections as:

$$A \Theta B = \bigcap_{b \in B} T_{-b}(A) \tag{4}$$

An important operator, which is the backbone of the pattern spectrum, is the *opening* morphological filter, defined as an erosion operation followed by a dilation using the same structuring element. The opening operator is defined as:

$$A \circ B = (A \Theta B) \oplus B \tag{5}$$

Dilation tries to undo erosion operation. However, some details closely related with the shape and size of the structuring element will vanish. Furthermore, an object disappearing as consequence of erosion cannot be recovered.

C*losing* morphological operator, which is the dual of the *opening*, is defined as dilation followed by an erosion operation using the same structuring element:

$$A \bullet B = (A \oplus B) \, \Theta B \tag{6}$$

Opening and closing filters have been used as discriminators for filtering, segmentation, edge detection, differential counting, or numerical analysis of shapes.

2.2 Morphological Pattern Spectrum

Pecstrum, or pattern spectrum of a compact binary image $A \subseteq R^2$, relative to a convex binary pattern $B \subseteq R^2$ called the *structuring element*, is defined as the differential size distribution function:

$$P_x(n,B)=\frac{dM(A\circ nB)}{dn},\quad n\geq 0 \tag{7}$$

where M represents the area measured in the intermediate operations, and nB is the n-times dilated structuring element. *Pecstrum* has the property of invariance to translation and rotation when B is an isotropic structuring element. Scale is determined by the size of the structuring element. The discrete version is given by:

$$P(n,B)=\frac{M[A\circ nB]-M[A\circ(n+1)B]}{M[A]} \tag{8}$$

Figure 2 shows the obtained pecstrum P(n) of a fractal image. It was calculated using a structuring element formed by a small circle with an initial size and incremental steps of 2 pixels.

Figure 3 shows the intermediate stages involved in the computation of the pattern spectrum between consecutive opening filters with an incremental structuring element according to the definition. The process concludes when the last image vanishes completely. It can be noticed also that the level of details filtered in each stage is closely related to the size of the structuring element.

Figure 4 shows the pattern spectra obtained from four ellipsoidal figures. It is relevant to point out that the pattern spectrum is able to represent quantitatively the geometric form when the horizontal axis of the ellipse increases. Given that the structuring element used in this experiment is a circle, there is only one spectral component when the two axes have the same length, i.e., when the input image is a circle itself.

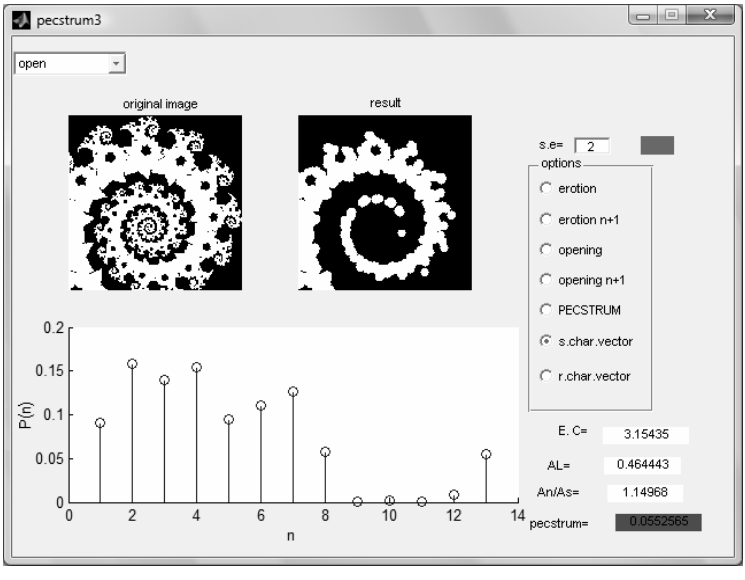

Fig. 2. Pattern spectrum of a fractal binary image.

As the horizontal axis increases some pattern spectral components arises, and the larger component, which is related to the center of the image, decreases. In any case the sum of all components always equals one, since the spectrum is normalized according to the definition.

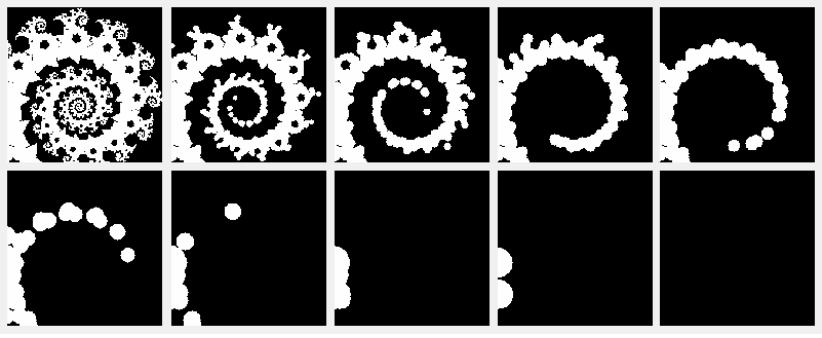

Fig. 3. Results obtained from intermediate opening filters with an incremental structuring element.

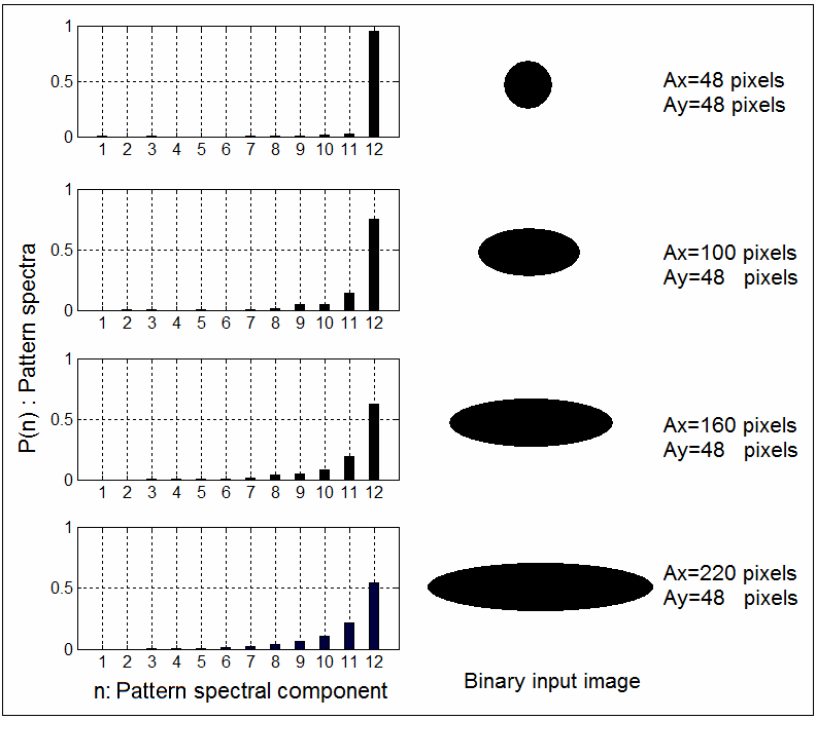

Fig. 4. Pattern spectra obtained from four ellipses increasing the major axis Ax.

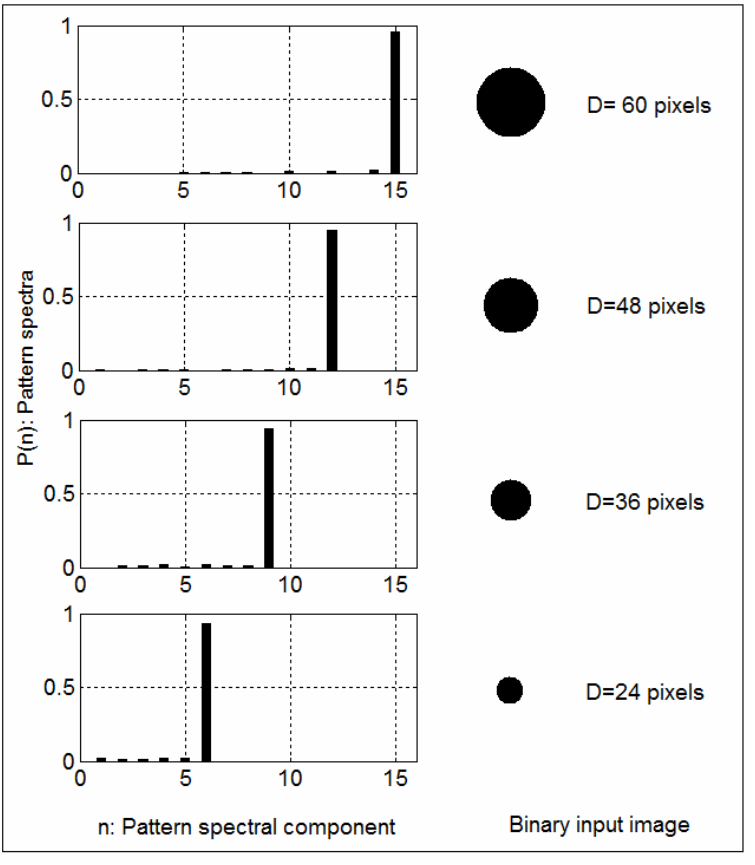

Fig. 5. Pattern spectra obtained from four circles with different diameter D.

The principal component located in the position n=12, indicates that the central part of the ellipses contains a circle of diameter D= 48 pixels. Figure 4 shows the situation in which the major axis Dx of the four ellipses consecutively increases while the minor axis remains without changes, and the result is reflected in the distribution of component in the pattern spectrum. Furthermore, figure 5 shows the case when the input image is a circle, and the diameter is increased with steps of 12 pixels. In that case there is only one component in the pattern spectrum, and the size is reflected in the position of the principal component. Some noise in the remaining pattern spectral components due to the shape and size of the structuring element can be distinguished.

These characteristics of the pattern spectrum clearly suggest the possibility of using it as a mathematical tool oriented to describe quantitatively the morphology of the white blood cells nuclei, which is the goal in the work presented in this paper.

3 Composed Feature Vector

A composed feature vector based on the cell morphological information is proposed as follows:

$$\vec{x} = \{A_L \vdots R_{nc} \vdots P(n,B)\} \tag{10}$$

where:

A_L = Leukocyte normalized area

R_{nc} = Nucleus-cytoplasm ratio

$P(n,B)$ = Pattern spectrum of the nucleus.

This vector contains information that in general human experts could consider to classify a leukocyte: Shape of the nucleus, represented by the pecstrum $P(n,B)$, relationship among the area of the cytoplasm and the area of the nucleus, represented by R_{nc}, and size of the cell, represented by A_L. Figure 6-a shows an image of a leukocyte, while figure 6-b shows the results obtained for the computation of the composed feature vector described before. The segmented image is plotted in the up-left part of figure 6-b. The obtained feature vector is plotted in the center of the figure, and the corresponding values are:

$$\begin{aligned}\vec{x} &= \{A_L \vdots R_{nc} \vdots P(n)\} \\ &= \{0.2700,\ 0.2878,\ 0.2709,\ 0.6216,\ 0.0858,\ 0.0075,\ 0.0009, 0.0, 0.0\}\end{aligned} \tag{11}$$

4 Multilayer Perceptron

The neural network model used in this work was a feedforward multilayer perceptron (MLP) with three layers of neurons: The input layer with nine neurons corresponding to the number of elements in the feature vectors, a hidden layer, and the output layer with six neurons corresponding each to a leukocyte class. By experimentation, FFNN architectures of (9-15-6) and (9-19-6) were found to fit best the data. When a multilayer perceptron network has *n* input nodes, one hidden-layer of *m* neurons, and two output neurons, the output of the network is given by [22]:

$$y_i = f_i\left(\sum_{k=1}^{m} w_{ki}\, f_k\left(\sum_{j=1}^{n} w_{kj}\, x_j\right)\right) \tag{12}$$

f_k, f_i: Activation functions of the hidden-layer and the output-layer neurons.

w_{ki}, w_{kj}: Weights connected to the output layer and to the hidden layer.

x_j: Input feature vector.

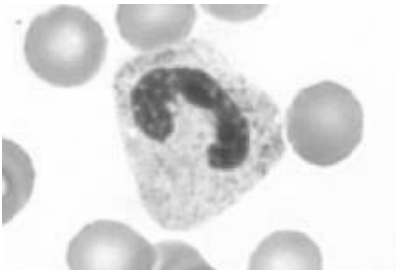

(a). original image

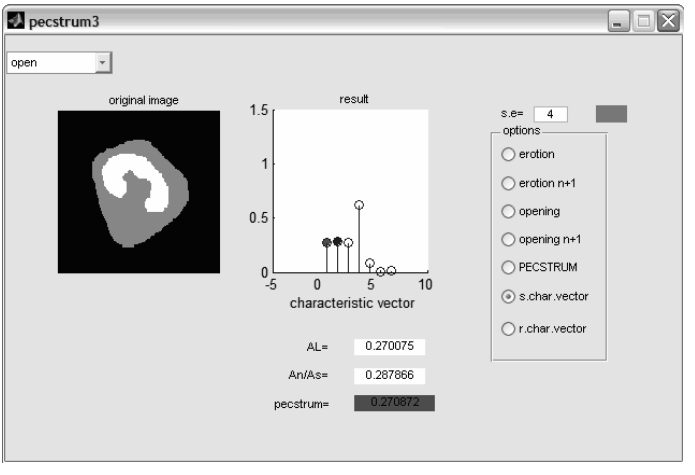

(b) Plot of composed feature vector

Fig. 6. An example of feature vector extraction

All neurons used a sigmoid as an activation function, expressed as:

$$f(u) = \frac{\alpha}{1 + e^{-bu}} \tag{13}$$

The feed forward multi-layer perceptron used in this work was trained using the Levenberg-Marquardt back propagation algorithm [23]. The backpropagation algorithm used in the training of multilayer perceptrons, is formulated as a non linear least-squares problem. Essentially, the Levenberg-Marquardt algorithm is a least-squares estimation method based on the maximum neighborhood idea. Let *E(w)* be an objective error function made up of *m* individual error terms e_i^2 *(w)* as follows:

$$E(w) = \sum_{i=1}^{m} e_i^2(w) = \left\| f(w) \right\|^2 , \tag{14}$$

where

$$e_i^2(w) = (y_{di} - y_i)^2 , \tag{15}$$

y_{di} is the desired value of output neuron i, and y_i is the actual output of that neuron. The aim of the Levenberg-Marquardt algorithm is to compute the weight vector w such as $E(w)$ is minimum. In each iteration the weight vector is updated according to eq. (6):

$$w_{k+1} = w_k + \delta w_k \ , \tag{16}$$

where

$$\delta w_k = -\left(J_k^T f(w_k)\right)\left(J_k^T J_k + \lambda I\right)^{-1} . \tag{17}$$

J_k is the Jacobian of f evaluated at w_k, λ is the Marquardt parameter, and *I* is the identity matrix. The number of epochs in the training phase differs from one example to another, however, the Levenberg-Marquardt back propagation algorithm provided consistently a fast convergence.

Figure 7 shows an example of training performance obtained in one of the experiments carried out with the data described in this work. It can be noticed that the goal was achieved in 30 epochs.

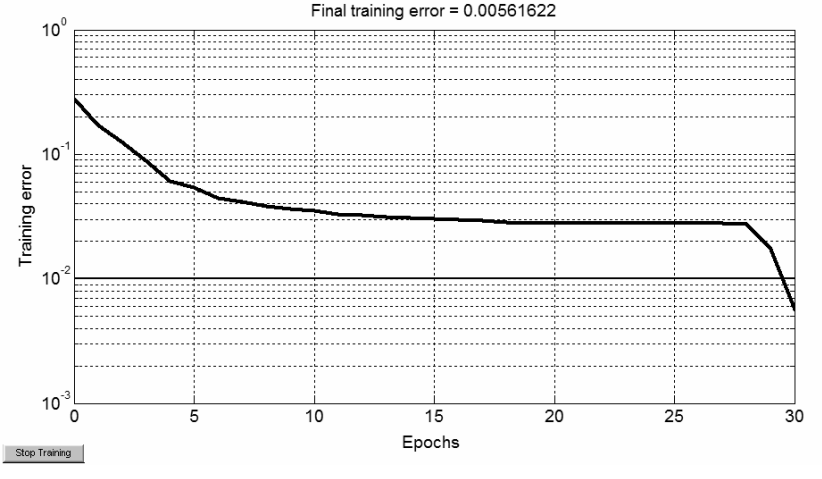

Fig. 7. An example of training performance

5 Support Vector Machines (SVM)

SVMs have been proposed for pattern recognition in a wide range of applications by its ability for learning from experimental data, and its effectiveness over some

other conventional parametric classifiers. Briefly, SVM is a statistical learning method based on a structural risk minimization procedure, which minimizes the upper bound of the generalization errors consisting of the sum of training errors and a confidence interval [24]. The original input space is transformed through a non-linear feature mapping to a high dimensional feature space, where the data is linearly separable by a hyperplane. The goal during the training process is to find the separating hyperplane with the largest margin in the obtained hyperspace. The transformation is performed using a non-linear function whose form is determined by some kernel. There are three common kernels used for the non-linear feature mapping: Polynomial, radial basis function, and sigmoid kernels. Linear hyperplane classifiers are based on the class of decision functions [25,26]:

$$y = sign\left((w^T x) + b\right) \tag{18}$$

The optimal hyperplane is defined as the one with the maximal margin of separation between the wo classes. The solution of a constrained quadratic optimization process can be expanded in terms of a subset of the training patterns called support vectors that lie on the margin:

$$w = \sum_{i=1}^{N} v_i x_i \tag{19}$$

Thus the decision rule depends only on dot products between patterns:

$$y = sign\left(\sum_{i=1}^{N} v_i (x_i \cdot x) + b\right) \tag{20}$$

The above linear algorithm is performed in the new feature space obtained through some non-linear transformation Ø by using some of the described kernels. The kernel is related to the Ø function by:

$$K(x_i, x) = \phi(x_i) \cdot \phi(x) \tag{21}$$

In this work the radial basis function (RBF) was used. RBF is defined as:

$$K(x_i, x_j) = e^{-\left\|x_i - x_j\right\|^2 / \sigma} \tag{22}$$

Classification of the test sample x is then performed by:

$$y = sign\left(\sum_{i=1}^{N} \alpha_i v_i K(x_i, x) + b\right), \tag{23}$$

where N is the number of training samples, v_i is the class label, α_i a Lagrangian multiplier, the elements x_i for which $\alpha_i > 0$ are the support vectors, and $K(x_i,x)$ is the function kernel. In this work a Gaussian radial basis function was used.

6 Experimental Description and Results

Input data was obtained from hand-segmented images of white blood cells in different maturity stages, some examples are shown in figure 8. Data set consists of 54 patterns corresponding to 7 artificial and 2 real images for each class. Artificial images were needed due to the lack of a public database to carry out the experiments. An artist generated the artificial segmented images hand-painting them in black and white pixels, using Paint. Figure 8-a shows examples of segmented real cells corresponding to each class, while figure 8-b shows examples of artificial cells. In order to test the performance of the proposed feature vector we used 4 different classifiers based on Euclidean distance, K-nearest neighbor (KNN), Feed-forward Neural Networks (FFNN) and Support Vector Machines (SVM) respectively. All classifiers were built using Matlab V 7.0. The FFNN was trained using the Matlab function ´trainlm´, which implements the Levenberg-Marquardt backpropagation training algorithm. SVM was extended to multi-class classification using the method known as DAGSVM (Directed Acyclic Graph Support Vector Machine) [25]. Matlab function ´svmtrain´ was used as a nucleus for the implementation of DAGSVM. The KNN was tested for k=1, 3 and 5. A statistical analysis of the obtained feature vectors is shown in Table 1. The table is organized by leukocyte type, showing means and variances of the feature characteristics for each class obtained from the dataset described before.

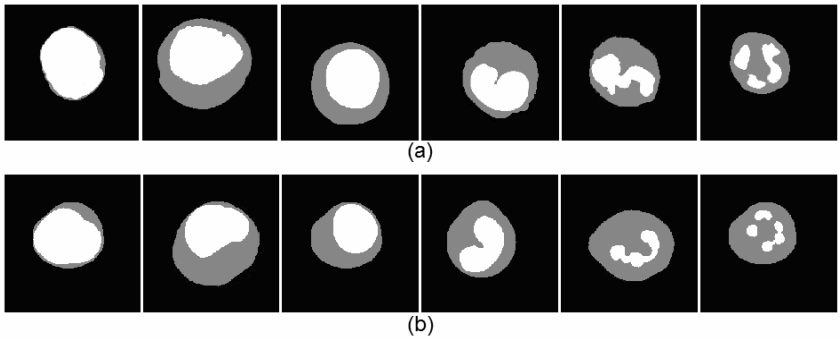

Fig. 8. Examples of patterns for each class, from left to right: Myeloblast, promyelocyte, myelocyte, metamyelocyte, band, and polymorphonuclear leukocytes (PMN). (a) Real images. (b) Artificial images.

It is interesting to analyze the plot of the mean feature vectors corresponding to each class. Figure 9 shows the feature vectors ordered according to the cell maturity stage from the youngest to the oldest. It can be noticed that the form of the feature vectors evolves by displacing the principal components to the right and decreasing their value at the same time.

Table 1. Mean and variance of composed feature vectors for the training data.

	A_L	R_n	P(1)	P(2)	P(3)	P(4)	P(5)	P(6)	P(7)
Leukocyte type:									
Myeloblast: Mean	0.1860	0.8347	0.8156	0.0726	0.0371	0.0124	0.0084	0.0074	0.0049
Variance	0.0203	0.0643	0.1005	0.0516	0.0162	0.0089	0.0062	0.0058	0.0031
Promyelocyte: Mean	0.2939	0.5075	0.841	0.0615	0.0361	0.0234	0.0114	0.0073	0.0046
Variance	0.0331	0.0029	0.0642	0.0158	0.0089	0.0183	0.0058	0.0046	0.0028
Myelocyte: Mean	0.2105	0.4984	0.9234	0.0336	0.0198	0.0091	0.0026	0.0026	0.0025
Variance	0.0321	0.0114	0.0254	0.0132	0.0049	0.0016	0.0018	0.0021	0.0003
Metamyelocyte: Mean	0.2048	0.4629	0.5170	0.3760	0.0678	0.0234	0.0070	0.0042	0.0026
Variance	0.0384	0.0136	0.0507	0.0751	0.0249	0.0035	0.0007	0.0008	0.0017
Band: Mean	0.2127	0.2028	0.5190	0.3510	0.1210	0.0088	0 .0	0.0	0.0
Variance	0.0226	0.0047	0.1691	0.1063	0.0601	0.0026	0 0	0.0	0.0
PMN: Mean	0.1796	0.1736	0.3893	0.4186	0.1573	0.0346	0.0	0.0	0.0
Variance	0.0198	0.0447	0.0179	0.0099	0.0398	0.0119	0 0	0.0	0.0

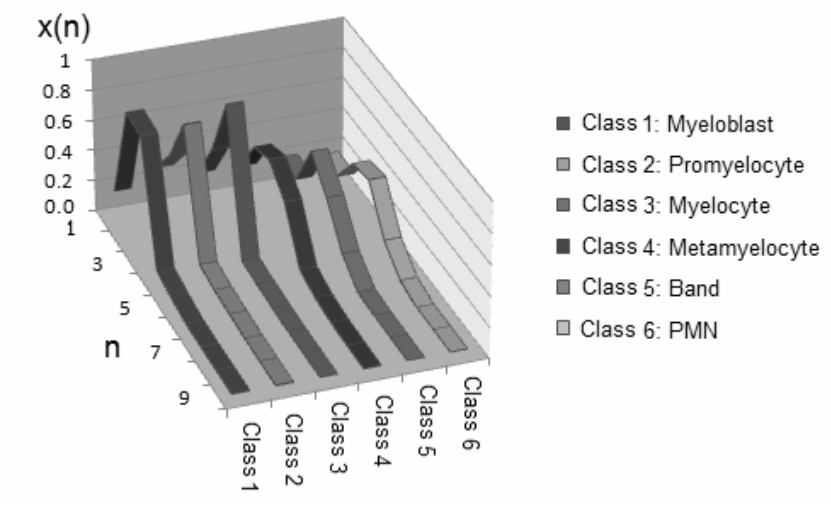

Fig. 9. Mean feature vectors corresponding to the six leukocyte classes

Table 2. Three-fold cross validation

Classifier	Classification Rate
Euclidean Distance	77.7%
K-NN with K= 1	70.4%
K-NN with K= 3	72.2%
K-NN with K= 5	70.4%
FFNN with 19 hidden nodes	**87.6%**
FFNN with 14 hidden nodes	84.9%
DAGSVM	71.6%

Three-fold cross validation was used to obtain the classification results shown in Table 2. Best results were obtained by a FFNN with 19 hidden nodes. A similar work reported a classification rate around 77%, [27] however, a fair comparison is not possible due to differences in the databases used.

7 Conclusions

A composed feature vector based on morphological information for classification of hand-segmented leukocytes images was presented. This feature vector was constructed with the morphological *pecstrum* as the central part, and some geometric considerations. The composed feature vector shows very good attributes to reflect the evolution in time of the white blood cells according to their maturity stage. The proposed feature extraction was tested using 4 different classifiers based on Euclidean distance, K-nearest neighbor (KNN), Feed-forward Neural Networks (FFNN) and Support Vector Machines (SVM) respectively. Three-fold cross validation was used to get the classification rates for each classifier. The best result was obtained by a FFNN with 19 hidden nodes, getting 87.6% of corrected classification. The reported work is part of an ongoing project on the cytology of human bone marrow images. The tools described in this paper will be used as the base for a second part in the project, oriented to the differential counting of white blood cells, and its use in the diagnosis and follow up of several pathologies, under the supervision of medical experts.

References

1. Butarello, M., Plebani, M.: Automated blood cell counts: State of the art. American Journal of Clinical Pathology 130, 104–116 (2008)
2. Araseki, K., Matsuda, A., Germing, U., Jinnai, I., Kuendgen, A., Iwanaga, M., Miyazaki, Y., Hata, T., Bessho, M., Gattermann, N., Tomonaga, M.: Differences in the distribution of subtypes according to the WHO classification 2008 between Japanese and German patients with refractory anemia according to the FAB classification in myelodysplastic syndromes. Leukemia Research 33(1), 66 (2009)
3. Bogdanovic, G., Jakimov, D., Stojiljkovic, B., Jurisic, V.: The cell growth, morphology and immunocytochemistry of novel cell line established from a bone marrow of the patient with therapy-related myelodysplastic syndrome. Medical Oncology 24(4), 419–424 (2007)
4. Germing, U., Aul, C., Niemeyer, C.M., Haas, R., Bennett, J.M.: Epidemiology, classification and prognosis of adults and children with myelodysplastic syndromes. Annals of Hematology 87(9), 691–699 (2008)
5. Jones, D.: Approaches to Classification of Lymphoma and Leukemia, book chapter on Neoplastic Hematopathology: Experimental and Clinical Approaches, pp. 3–20. Humana Press, Totowa (2010)
6. Mayumi-Ushizima, D., Costa-Rosatelli, M.: E-Learning in Medical Diagnosis. In: Proceedings of 16th Brazilian Symposium on Computer Graphics and Image Processing, Natal, Brazil (2005)

7. Kang, S.H., Kim, H.K., Ham, C.K., Lee, D.S., Cho, H.I.: Comparison of four hematology analyzers, CELL-DYN Sapphire, ADVIA 120, Coulter LH 750, and Sysmex XE-2100, in terms of clinical usefulness. International Journal of Laboratory Hematology 30(6), 480–486 (2007)
8. Piuri, V., Scotti, F.: Morphological classification of blood leukocytes by microscope images. In: Proceedings of IEEE International Conference on Computational Intelligence for Measurement Systems and Applications Boston, Boston, MD, USA, July 14-16 (2004)
9. Chen, Q., Fan, Y., Udpa, L., Ayres, V.: Cell classification by moments and continuous wavelet transform methods. International Journal of Nanomedicine 2(2), 181–189 (2007)
10. Theera-Umpon, N.: White Blood Cell Segmentation and Classification in Microscopic Bone Marrow Images. In: Wang, L., Jin, Y. (eds.) FSKD 2005. LNCS (LNAI), vol. 3614, pp. 787–796. Springer, Heidelberg (2005)
11. Dorini, L.B., Neucimar, R.M., Leite, J.: White blood cell segmentation using morphological operators and scale-space analysis. In: Proceedings of XX Brazilian Symposium on Computer Graphics and Image Processing, Belo Horizonte, Brazil, October 7-10, pp. 294–301 (2007)
12. Shih, F.Y.: Image processing and mathematical morphology: Fundamentals and applications. CRC Press, Taylor and Francis Group (2009)
13. Ledda, A., Philips, W.: Majority Ordering and the Morphological Pattern Spectrum. In: Blanc-Talon, J., Philips, W., Popescu, D.C., Scheunders, P. (eds.) ACIVS 2005. LNCS, vol. 3708, pp. 356–363. Springer, Heidelberg (2005)
14. Maragos, P.: Pattern spectrum and multiscale shape representation. IEEE Transactions on Pattern Analysis and Machine Intelligence 11, 701–716 (1989)
15. Pitas, A., Venetsanopoulus, A.N.: Non-linear Digital Filters; Principles and Applications. Kluwer Academic Publishers, Norwell (1990)
16. Yunpeng, L., Fangcheng, L., Chengrong, L.: Pattern recognition of partial discharge based on its pattern spectrum. In: Proceedings of International Symposium on Electrical Insulating Materials, Kitakyushu, Japan (2005)
17. Ghosh, D., Tou Wei, D.C.: Material Classification Using Morphological Pattern Spectrum for Extracting Textural Features from Material Micrographs. In: Narayanan, P.J., Nayar, S.K., Shum, H.-Y. (eds.) ACCV 2006. LNCS, vol. 3852, pp. 623–632. Springer, Heidelberg (2006)
18. Ledda, A., Samyn, P., Quintelier, J., De Baets, P., Philips, W.: Polymer Analysis with Mathematical Morphology. In: Proceedings of IEEE Benelux Signal Processing Symposium, Hilvarenbeek, The Netherlands, pp. 87–92 (2004)
19. Omata, M., Hamamoto, T., Sangai, S.: Lip recognition using morphological pattern spectrum. In: Proceedings of Third International Conference on Audio- and Video-Based Biometric Person Authentication, Halmstad, Sweeden, pp. 108–114 (2001)
20. Theera-Umphon, N., Dhompongsa, S.: Morphological Granulometric Features of Nucleus in Automatic Bone Marrow White Blood Cell Classification. IEEE Transactions on Information Technology in Biomedicine 11(3), 353–359 (2007)
21. Ramirez-Cortes, J.M., Gomez-Gil, P., Sanchez-Perez, G., Prieto-Castro, C.: Shape based hand recognition approach using the pattern spectrum. Journal of Electronic Imaging 18(1), 013012, 1–6 (2009)
22. Haykin, S.: Neural networks and learning machines, 3rd edn. Pearson, Prentice Hall, New Jersey (2009)

23. Demuth, H., Beale, M., Hagan, M.: Neural Network Toolbox 6 User's guide. The MathWorks, Inc., 5-30, 5-33 (2009)
24. Burges, C.J.C.: A tutorial on support vector machines for pattern recognition. Data Mining and Knowledge Discovery 2, 121–127 (1998)
25. Scholkopf, B., Smola, A.J.: Learning with kernels: support vector machines, regularization, optimization, and beyond, pp. 189–211. MIT Press, Massachussetts (2002)
26. Abe, S.: Support Vector Machines for Pattern Classification. Springer, Heidelberg (2005)
27. Theera-Umpon, N., Gader, P.D.: Counting white blood cells using morphological granulometries. Journal of Electronic Imaging 9(2), 170–177 (2000)